

● *Original Contribution*

MONITORING OF CELL DEATH IN EPITHELIAL CELLS USING HIGH FREQUENCY ULTRASOUND SPECTROSCOPY

SEBASTIAN BRAND,^{*†||} BINDIYA SOLANKI,[‡] DEBORA B. FOSTER,[‡] GREGORY J. CZARNOTA,^{†§||}
and MICHAEL C. KOLIOS^{†||}

^{*}Ontario Cancer Institute, Princess Margaret Hospital, Toronto, Ontario, Canada; [†]Department of Physics, Ryerson University, Toronto, Ontario, Canada; [‡]Department of Chemistry and Biology, Ryerson University, Toronto, Ontario, Canada; [§]Department of Radiation Oncology, Sunnybrook Health Sciences Center, University of Toronto, Toronto, Ontario, Canada; ^{||}Department of Medical Biophysics, University of Toronto, Toronto, Ontario, Canada; and ^{||}Q-BAM Laboratory, University of Halle, Halle, Germany Toronto, Ontario, Canada; Halle, Germany

(Received 21 April 2008; revised 9 September 2008; in final form 17 September 2008)

Abstract—Spectral and wavelet analyses were performed on ultrasound radiofrequency (RF) data collected from centrifuged cell samples containing HEP-2 cells after induction of apoptosis by exposure to camptothecin. Samples were imaged at several time points after drug exposure using high-frequency ultrasound in the range from 10–60 MHz. A 20-MHz transducer with a f-number of 2.35 and a 40-MHz transducer with a f-number of 3 were used for collecting the RF data. Normalized power spectra were computed from the backscattered ultrasound signals within a region-of-interest (ROI) for further analysis. Spectral slopes, integrated backscatter coefficients (IBCs) and wavelet parameters were estimated as a function of treatment time to monitor acoustic property changes during apoptosis. Changes in spectral parameters were detected starting six hours after treatment and coincided with changes in corresponding histology. Throughout the course of chemotherapy, variation in estimates of the spectral slope of up to 35% were observed. During the treatment, IBCs increased by 400% compared with estimates obtained from the control samples. Changes in spectral parameters are hypothesized to be linked to structural cell changes during apoptosis. In addition, the sensitivity of a wavelet-based analysis to the ultrasonic assessment of cellular changes was investigated. Results of the wavelet analysis showed variations similar to the spectral parameters. Where values of the spectral slope decreased, estimates of the scaling factors increased. Because wavelet analysis preserves the signal–time localization, its application will be potentially beneficial for assessing treatment responses *in vivo*. The current study contributes toward the development of a non-invasive method for monitoring apoptosis as a measure of the success of chemotherapeutic treatment of cancer. (E-mail: Sebastian.Brand@gmail.com) © 2009 World Federation for Ultrasound in Medicine & Biology.

Key Words: High-frequency ultrasound, Quantitative ultrasound, Spectral analysis, Wavelet analysis, HEP-2 cells, Apoptosis, Ultrasound backscatter, Cancer treatment efficacy.

INTRODUCTION

Ultrasound is one of the most commonly used imaging modalities in medical diagnostics. However, typically only the magnitude of the envelope of the ultrasound echoes is used to generate greyscale backscatter images. Investigators have shown that the frequency-dependent information in ultrasound backscatter can be related to acoustical and structural properties of tissue microstructure (Feleppa et al. 1986; Insana et al. 1990; Lizzi et al.

1986, 1997a; Nicholas 1982). Spectral analysis of the radiofrequency (RF) ultrasound echo signals can provide information about the tissue properties like attenuation (Madsen et al. 1999), backscattering strength as a function of frequency (Waters et al. 2003) and effective scatterer size (Lizzi et al. 1983; Oelze et al. 2004b; Oelze et al. 2006). For frequencies <15 MHz, tissue characterization using ultrasound has been studied extensively in the last decades. Signal properties estimated from ultrasound backscatter of biological tissues were shown to provide additional information about tissue pathology (Huisman et al. 1998; Lizzi et al. 1988; Romjin et al. 1989) and this information is typically presented as a parametric image superimposed on a B-scan image.

Address correspondence to: Dr. Sebastian Brand, Martin-Luther University of Halle, Department of Orthopaedics, Q-BAM Laboratory, Magdeburger St. 22, 06112 Halle/S, Germany. E-mail: Sebastian.Brand@gmail.com

However, until recently, the lack of studies that demonstrated an added clinical value from such parametric images had resulted in reduced interest in the pursuit of such methods.

Because the relatively recent developments in high-frequency ultrasound transducers and fast analog-to-digital converters (ADC), several groups have worked on tissue characterization in the range between 20 and 80 MHz (Bridal *et al.* 1997; Cloutier *et al.* 1997; Foster *et al.* 2000; Silverman *et al.* 1995, 2001; Saied *et al.* 2004; Ursea *et al.* 1998; Vogt *et al.* 2003). As the ultrasound wavelength approaches the cell size, it is expected that ultrasonic techniques will be more sensitive to structural changes at the cell level, such as those seen during apoptosis. High-frequency ultrasound tissue characterization has shown great discriminatory power in the ultrasound imaging of mouse tumors (Oelze *et al.* 2002; Mamou *et al.* 2005; Tunis *et al.* 2005), plaque formation (Nair *et al.* 2001) and the formation of aggregates in blood (Yu *et al.* 2007). Conventional ultrasound characterization techniques, such as the use of spectral parameters (Lizzi *et al.* 1983) have been used in the aforementioned studies. However, more complex algorithms and theoretical models have to be developed to increase the sensitivity of these techniques to subtle structural changes in tissue. Oelze *et al.* (2003, 2004b, 2006) have used estimates of the scatterer size and acoustic concentration to increase the sensitivity to the tumor microstructure for the differentiation of fibroadenoma and carcinomas. Nair *et al.* (2001) have used the spectral slope, midband fit and autoregressive spectral models for the classification of intravascular plaques.

We have previously demonstrated that changes at the cellular level induced by exposure to chemotherapeutic drugs can be detected using high-frequency ultrasound (Czarnota *et al.* 1997, 1999; Kolios *et al.* 2002). Individual cells cannot be resolved in the frequency range from 10–60 MHz; however, changes in backscatter intensity and spectral parameters from cell ensembles can be observed. In these previous studies, acute myeloid leukemia cells (AML) were used. These cells, which are not epithelial cells, can grow rapidly in suspension, and therefore permit the growth of large quantities of cells. Those studies showed that the backscatter intensity increased during apoptosis. We hypothesize that the changes in the nuclear structure observed during apoptosis are partly responsible for the increase in backscatter. Our hypothesis is based on the fact that the size of the nucleus has been shown to correlate well with the frequency-dependent backscatter intensity in highly cellular systems by Taggart *et al.* (2007).

An interesting alternative to the conventional spectral analysis has been reported by Georgiou *et al.* (2000, 2001). In those studies, a wavelet analysis of the RF data were

performed to extract parameters related to the microstructure of breast tissues (including carcinomas). The tissue classification was based on signal parameters derived from the coherent and the diffuse components of backscattered ultrasonic signals. Whereas the diffuse component reflects the texture of the echo created from the large number of randomly located unresolvable scatterers, the coherent signal component contains information about the resolvable scatterers in the resolution cell. It was found that this wavelet technique permitted the differentiation of normal, fibroadenoma and fibrocystic tissue from each other. Wavelet analysis offers several advantages over spectral analysis. One of them is related to the fact that any individual wavelet in a wavelet analysis is located in time (and consequently space), whereas the sine and cosine components in a Fourier analysis are not. To allow for localization in a Fourier analysis, short-time Fourier transform (STFT) can be used. However, it requires the use of a fixed window size, which leads to a fixed time–frequency resolution, ultimately resulting in a trade-off between resolution and localization (Graps 1995). A wavelet analysis could therefore be used for the spatial discrimination of tumor volumes responding to treatment *vs.* volumes not responding.

In the present work, we investigate the sensitivity of spectral methods to changes in a human epithelial carcinoma cell line (HEp-2) induced by camptothecin treatment. This cell line was chosen for the current study because it is closer than the previously used AML cell line, to the cell type found in solid tumors. Since *in vivo* detection of those changes might require accurate localization and good spectral resolution, which are not necessarily provided by STFT, the wavelet analysis technique is also investigated.

The wavelet transform was applied to the RF signals to investigate the sensitivity of a wavelet-based analysis method toward the detection of apoptosis. We examined the variation of signal parameters as a function of time after drug exposure. The results of the spectral analysis were compared with results of the wavelet analysis.

The cell line investigated in this study is a human epithelial carcinoma cell line (HEp-2). Camptothecin was applied to induce apoptosis, which effects the nuclear enzyme Topoisomerase I (Dancey *et al.* 1996; Donehower *et al.* 1993; Li *et al.* 1972; Shinka *et al.* 1995) and inhibits the DNA religation. This causes the cells to trigger the apoptotic death sequence. The most ubiquitous characteristics of apoptosis are cell shrinkage, formation of cell surface blebs (caused by the separation of the plasma membrane and the cytoskeleton) and the formation of apoptotic bodies. Apoptotic bodies are cellular fragments created during the apoptotic process that contain the condensed cell content. *In vivo* apoptotic

bodies are dissolved rapidly by macrophages (Doonan et al. 2008).

MATERIALS AND METHODS

Cell samples

Human squamous laryngeal carcinoma cells (HEp-2 from the American Type Culture Collection, Manassas, VA, USA) were used in the experiments. HEp-2 is a p53 mutated cell line and is known to respond to camptothecin by inducing apoptosis (Jones et al. 2000; Taron et al. 2000). Cells were cultured in minimum essential media (MEM) supplemented with 10% of heat-inactivated fetal bovine serum (FBS) and 0.1% gentamycin (antibiotic) in a humidified atmosphere at 37° C containing 5% CO₂. For each experiment, cells were taken from a frozen stock were thawed and then cultured in cell culture flasks containing 15 ml of the described medium. Apoptosis was induced in HEp-2 cells by adding camptothecin into the medium of each flask resulting in a total concentration of 30 µg/ml. Camptothecin is part of a relatively new class of chemotherapeutic agents that target the nuclear enzyme Topoisomerase I (Topo I) (Dancey et al. 1996; Donehower et al. 1993; Li et al. 1972). By inhibiting the enzyme Topo I, the number of covalent Topo I-DNA complexes increases and leads to the formation of double-strand DNA breaks (Kaufmann et al. 1996) and, ultimately, apoptosis.

Before ultrasonic data acquisition, HEp2 cells were exposed to camptothecin for 3, 6, 17, 21, 24, 30 and 48 h. After this chemotherapeutic treatment, the adherent HEp2 cells were detached from the cell culture flask using trypsin and centrifuged at 216 g. Then the cell culture medium was removed. Cells were resuspended in phosphate-buffered saline (PBS) and centrifuged at 1942 g, resulting in the final centrifuged sample. The samples had a diameter of 8 mm and a height of approximately 5 mm. For ultrasound experiments, cell samples were immersed in PBS, which acted as the coupling medium for the acoustic wave propagation. All ultrasonic investigations were finished within 30 min after the final centrifugation.

After ultrasonic imaging, cell samples were fixated in 10% (w/v) formalin in phosphate-buffered saline (PBS), embedded in paraffin and processed for hematoxylin and eosin (H&E) staining. H&E is a stain commonly used in histology, staining the nucleic acids purple and the protein contained in the cytoplasm pink. Eosin (negatively charged) interacts with positively-charged cytoplasmic proteins, resulting in bright pink staining, whereas hematoxylin (positively charged) combines with the negatively-charged phosphate groups of the nucleic acids, staining them blue (Doonan et al. 2008). The morphology of the cells was analyzed using light micros-

Table 1. Specifications of the ultrasound transducers used for the high-frequency ultrasound experiments

Transducer description	20 MHz	40 MHz
Center frequency (f_c)	19.25 MHz	37.5 MHz
-6 dB (bandwidth)	100%	98%
f-number	2.35	3
Diameter of transducer aperture (mm)	8.5	3
Depth of focus (mm)	3.2	2.5
FWHM (lateral) (µm)	247	157
Pulse length (ns)	110	50

copy, which was performed using a Zeiss Axioscope 20 (Carl-Zeiss, Oberkochen, Germany). The microscope included a CCD camera, which was used to record digital microscopy images.

Ultrasonic data acquisition and signal analysis

Ultrasonic imaging and RF data acquisition was performed with a high-frequency ultrasound device (UBM) (VS40B, VisualSonics Inc., Toronto, ON, Canada). Two single-element transducers were used for the experiments, a 20-MHz and a 40-MHz transducer (VisualSonics Inc.). A detailed description of the transducer specifications is given in Table 1. Bandwidth values are stated for the -6 dB range relative to the center frequency in the power spectrum. The use of two transducers expands the analysis frequency range from 10–60 MHz and allows verifying the independence of the results from the system transfer characteristics of the instrument. The ultrasonic device enabled real-time B-mode imaging of the interrogated specimen. The sampling frequency of the UBM's built-in analog-to-digital converter unit was 500 MS/s (input range: ±250 mV; digitizing resolution: 8 bit).

Ultrasound scanning was performed on two centrifuged cell samples at each time point. One of the samples contained untreated HEp-2 cells as a control and the other contained camptothecin-treated HEp-2 cells. The entire set of experiments was repeated to investigate experimental reproducibility. A total of 150 RF scan lines were acquired from three different scan planes (50 lines per scan plane). To obtain uncorrelated signals, scan lines and scan planes were separated by a distance of 250 µm, which is larger than the beamwidth of each of the transducers used. The length of the recorded RF data segments was 3–4 mm (Fig. 1–left) containing features of the sample container. Acquired data segments were positioned around the focus of the transducer, which was consistently placed 1–2 mm below the cell sample surface.

Signal analysis was performed using a custom-made software developed using MATLAB (The MathWorks, Natick, MA, USA). This software performed the image reconstruction, for 2-D visualization of the raw RF

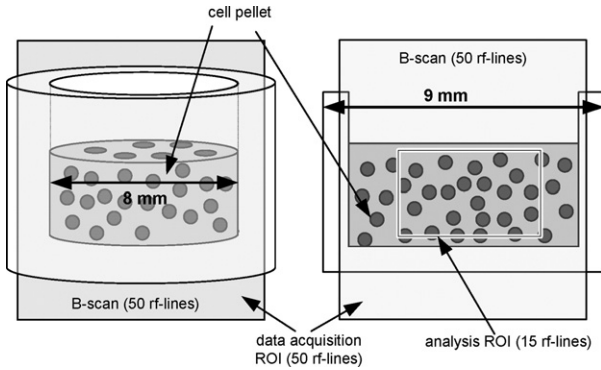


Fig. 1. Illustration of data acquisition. (a) Schematic of a cell sample inside the container. Gray area indicates where the data for the B-scan were acquired. This region contains 50 RF lines. The spacing between the cells is for illustrative purpose only. (b) Gray indicated area shows the B-scan acquired. The white ROI inside marks the region where RF data were chosen for spectral and wavelet analysis.

data and allowed the selection of ROIs. Three ROIs (1 per scan plane), each containing 15 RF lines, were selected from each cell sample at each time point. They were inside the cell sample, 1 mm in depth, and centered at the focus. Fourier and wavelet analyses were performed on each individual RF data segment in the ROI, using functions from the MATLAB signal processing and wavelet toolboxes. Parameter estimates were obtained by averaging results from the computation of the 45 uncorrelated RF data segments.

Spectral analysis

Before parameter computation spectra were compensated for attenuation, effects of the diffraction pattern and effects of signal-windowing. In preparation for the Fourier transform, RF time signals were gated by applying a rectangular window function. The window length was 400 ns, which corresponds to eight wavelengths at 20 MHz and 16 wavelengths at 40 MHz. Wavelength estimates are computed using the transducer's central frequency and the sound velocity inside distilled water at 21° C (1485 m/s) (Briggs 1992). Edge effects on the signal spectrum, induced by applying a rectangular window function, were minimized by using an algorithm proposed by Oelze *et al.* (2004a). Because gating of a time signal creates unwanted frequency components, spectral estimates are biased. Oelze *et al.* (2004a) have developed a compensation algorithm accounting for effects occurring when applying a rectangular time-gate. Attenuation along the path of sound propagation through the coupling medium was compensated for frequency dependence using an attenuation coefficient of 2.26×10^{-4} dB/(MHz² mm) (Briggs 1992).

Attenuation compensation inside cell samples was

done using values obtained by measuring the frequency-dependent attenuation of the cell samples. For untreated cells, values were calculated based on the reflection amplitudes obtained from a quartz reflector (part 43424, Edmund Industrial Optics Inc., Barrington, NJ, USA) that replaced the bottom of the cell sample holder. These values were normalized to the cell sample thickness. The attenuation measured in untreated cell samples was 0.015 dB/(MHz mm) and 0.057 dB/(MHz mm) for the 20 MHz and 40 MHz transducer, respectively. The details of the method applied for estimating cell sample attenuation can be found elsewhere (Brand *et al.* 2008). Attenuation compensation in the treated cell samples was performed using attenuation values calculated for each time point and transducer (Table 2). Treatment-dependent attenuation values were estimated using the frequency-dependent amplitude decrease over depth of the samples investigated (Jenderka *et al.* 1990; Lu *et al.* 1999). RF signals recorded from treated cell samples were analyzed independently for each time point. After compensating for transducer-specific diffraction effects, the slope of the spectral amplitudes over depth at 63 individual frequencies (within the -6 dB bandwidth) of each transducer was calculated.

To compensate for the diffraction effects associated with the source geometry, RF data collected from untreated HEp2 samples were used to derive a depth and frequency-dependent diffraction correction function (Gaertner *et al.* 1996; Jenderka *et al.* 1999). Spectra of the signals included in a window (applying the same settings as for the gating of the RF signals), which was progressively shifted by 80 μ m along the axis of the transducer, were calculated. Assuming homogeneity of the cell sample as a function of depth, *i.e.*, assuming a scattering cross section and distribution constant over depth, the normalization of these spectra by the spectrum obtained from the window at the focus removed any frequency-dependent transfer function related to the transmit and receive subsystem of the ultrasound device, including the transmit electrical pulse. The normalized spectra were then corrected for the attenuation (Table 2; 0h) along the propagation path in the cell sample, to obtain a diffraction correction expressed as a function of

Table 2. Attenuation values used for compensating treatment-dependent attenuation

α (dB/[MHz cm])	0 h	3 h	17 h	21 h	24 h	30 h	48 h
20 MHz	0.149	0.15	0.156	0.17	0.19	0.21	0.17
40 MHz	0.57	0.60	0.67	0.77	0.72	0.81	0.67

The values of untreated cells were estimated from the reflection of a flat quartz surface behind the cell sample. Treatment-dependent variations were estimated from the depth and spectral dependent decrease of the recorded RF signals after compensation for diffraction effects.

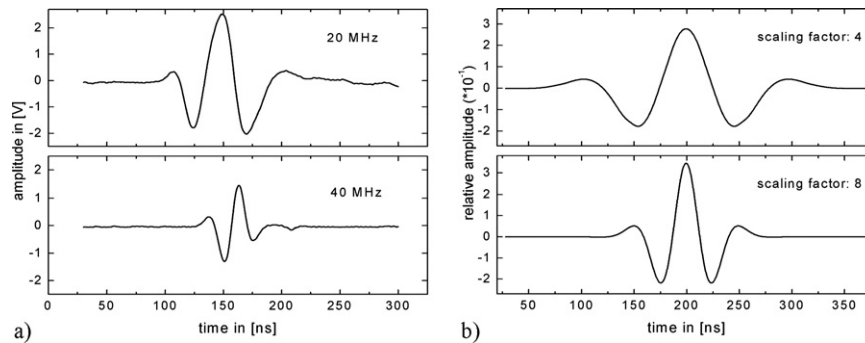


Fig. 2. (a) Reference pulses of the 20 MHz and 40 MHz transducer recorded from a quartz plate at the transducer's focus. (b) Gaussian wavelet of the fourth order as provided by the MATLAB wavelet toolbox. Scaled with the factor 4 (top) and factor 8 (bottom).

depth and frequency. Because compensation functions were required for each individual transducer, attenuation compensation was performed separately for each transducer using the corresponding values, discussed before. This diffraction correction function was then used to normalize all spectra obtained from treated and untreated cell samples, which were previously corrected treatment-time specific for attenuation.

To compensate for the transfer properties of the ultrasonic equipment, all power spectra were normalized to the reflection of a flat quartz reference (Lizzi 1997b, 1997c), placed at the focus of the transducer. In Fig. 2a signals reflected from the reference material with the surface at the transducers focus (quartz-glass cylinder [part 43424], Edmund Industrial Optics Inc., Barrington, NJ, USA), are presented. Application of this normalization was performed after compensating for attenuation and diffraction effects and removed the frequency-dependent transfer characteristics of the transmit–receive subsystem in addition to the transmit electrical pulse from the spectra obtained from treated and untreated cell samples. Linear regression analysis was applied to the normalized power spectra within the -6 dB frequency range of the reference spectrum. After compensation for the transfer properties of the entire system (including the electrical and acoustical subsystem) the slope of the normalized power spectrum can be directly related to the average scatterer size. The integrated backscatter coefficients (IBCs) were derived from the normalized power spectra using an algorithm described elsewhere (Turnbull et al. 1982; Worthington et al. 2001). The IBCs estimated after compensation for the system characteristics is related to the number density of the scatterers and the mismatch in acoustic impedance relative to the scattering background.

Wavelet analysis

Wavelet analysis is a 2-D signal transformation, which overcomes the main weaknesses of the STFT. The

application of a static window length as used in STFT results in a constant time and frequency resolution of the transformed signal. In the wavelet analysis, the analyzing wavelet is expanded and compressed in addition to sliding over the signal analyzed. This adaptation results in an improved temporal and spectral resolution, which cannot be obtained by a Fourier transformation (Graps et al. 1995). During scaling of the analyzing wavelet, the number of oscillations of the wavelet remains constant, resulting in a variation of the spectral content. Wavelet analysis of a signal computes coefficients at different scaling factors describing the correspondence between the analyzing wavelet and the signal. For illustration, a wavelet coefficient corresponds to the area below the result of a multiplication of the analysis wavelet and the signal at a particular wavelet scaling. Although the STFT provides a complex coefficient for one parameter (frequency), the continuous wavelet transform (CWT) computes one coefficient for each combination of the scaling factor and the temporal position.

The wavelet transformation performed in the current study used the MATLAB functions for the CWT. A Gaussian wavelet of the fourth order was chosen because of its similarity to the ultrasonic pulses used in the experiments. For illustration, the reference pulses are plotted together with the Gaussian wavelet in Fig. 2. The analyzing wavelet in Fig. 2b was scaled with the factors 4 and 8 to show how the mother wavelet changes when adapting the scaling factors during the wavelet analysis. The number of cycles inside the wavelet remains constant at different scaling conditions, influencing its spectral characteristics. As with the Fourier transform as described before, the CWT was applied to each scan line within the ROI.

However, compensation of system-dependent transfer properties of the ultrasonic equipment and compensation for attenuation has not been conducted so far for the CWT analysis. From the computation, the maximum wavelet coefficients and the corresponding scaling fac-

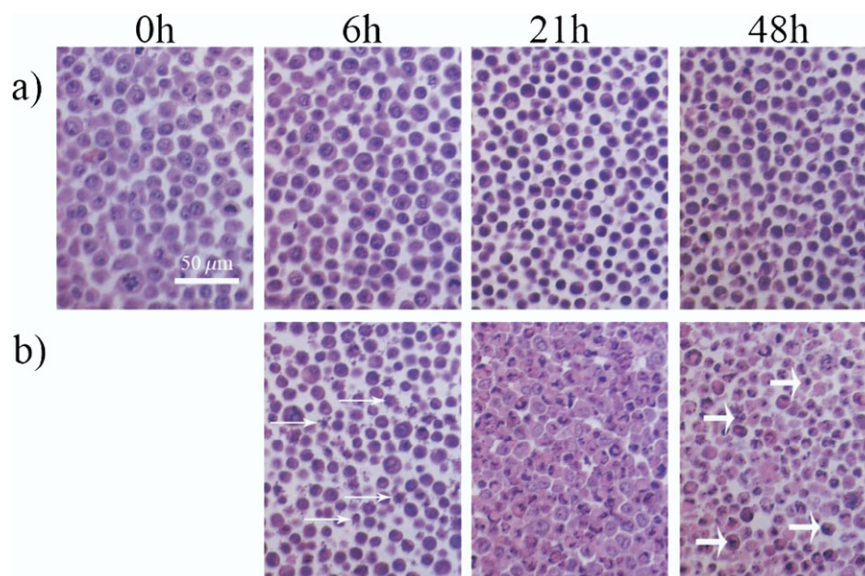


Fig. 3. Images of H&E-stained HEp-2 cells at different time points after treatment with camptothecin using light microscopy. (a) Untreated cell samples for control; (b) treated cell samples. Arrows (thin) point to membrane blebbing typically seen during apoptosis, and arrows (thick) indicate areas of nuclear condensation and margination. Cell diameters decreased from 15 μm at 0 h to 8 μm at 48 h.

tors were computed, averaged within the ROI and analyzed as a function of treatment time. The maximum wavelet coefficient (MWC) can be related to the amplitude in the spectrum, representing the energy of the underlying signal. As described previously, the expanding/compressing of the analyzing wavelet influences its spectral content that leads to the relation between the scaling factors obtained from the wavelet analysis and the center frequency of the signal of interest in the spectral analysis. Therefore, in regions with higher acoustic concentration, higher values for the wavelet coefficient are expected. The scaling factor on the other hand is expected to vary with the effective scatterer cross section so that decreasing values of the coefficient would be anticipated when scatterer sizes decrease. However, these results may properly be interpreted only when a careful compensation of the transfer properties is performed.

RESULTS

Histology and microscopy

Figure 3 contains optical micrographs of HEp-2 cells stained with H&E. The upper row in Fig. 3a shows the H&E histology of samples containing untreated HEp-2 cells at four treatment times. These images show the normal morphologic variations of the investigated cell line during the cell cycle (control experiment). Differences in those images of the untreated cells are caused by cell cycle-dependent staining variations. In the sec-

ond row (Fig. 3b), optical micrographs of HEp2 cells at different treatment times after exposure to camptothecin are presented (treatment experiment). A change in intra- and intercellular structure can be seen clearly after six hours of drug exposure, with apoptotic bodies (nuclear fragmentation) occurring.

Characteristic features of apoptosis including chromatin condensation and margination, membrane blebbing and cell shrinkage are evident when comparing Fig. 3a and b. The results indicate that the major structural changes associated with exposure to camptothecin occur between 6 h and 30 h of treatment. Visual inspection of the H&E histology in Fig. 3 provides information about changes of cell size and nuclear fragmentation.

Ultrasound imaging and spectroscopy

Ultrasound B-mode scans of treated and untreated HEp-2 cell samples are provided in Fig. 4 as a sequence over treatment time. These images (containing 255 scan lines) represent the size of the cell sample, which was approximately 8 mm (width) by 3 mm (height) and were recorded using a 20 MHz transducer. The changes in image brightness represent differences in the intensity of the backscattered ultrasound (all acquisition settings were identical). Significant changes in ultrasound image brightness occur at the same experimental times when changes in histology can be detected. To quantify those changes, spectral and wavelet parameters were estimated and plotted vs. time in Figs. 6–9. The data plotted in the

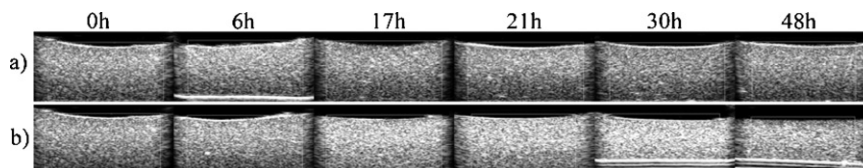


Fig. 4. Ultrasound B-scan images of samples containing HEP-2 cells at different time points after treatment with camptothecin recorded with the 20 MHz transducer. (a) Untreated cell samples; (b) treated cell samples. System settings were the same for all scans. Images are 3×8 mm in size.

figures represent the mean values calculated from the different ROIs analyzed ($n = 3$ in each cell sample). The error bars express the standard deviation of these parameters at each time point. Means and standard deviations were estimated from the mean values computed from the echo signals within each of the three ROIs. The two groups of data points for control and treated cells in the figures represent the experiment repeated (labeled “2”) two weeks after the first experiment (labeled “1”).

Characteristic normalized power spectra of treated and untreated HEP-2 cell samples calculated from the signals collected with both the 20 and 40 MHz transducers are shown in Fig. 5. The overlap of the normalized power spectra in the frequency range, which is common to the bandwidths of the two transducers, demonstrates that all frequency-dependent corrections were applied adequately to the collected raw RF signals. This has been observed for all cell samples. Linear fits obtained in the bandwidth of each transducer are also shown. The data in Fig. 5 demonstrate that although significant differences in the frequency-dependent backscatter properties between treated and untreated cells can be detected at 20 MHz, this difference in backscatter is greatly reduced when using the 40 MHz transducer to image the exact same sample. In both cases, however, there is a significant change in spectral slope.

Figure 6 shows the variations of the normalized spectral slopes obtained at 20 MHz (a) and 40 MHz (b) as a function of the duration of the exposure to the drug. The spectral slopes at times greater than six hours decrease for samples containing treated HEP-2 cells. Small but consistent changes in the spectral slopes of the untreated cells were also measured. In Fig. 6b, the spectral slopes for the same-cell samples scanned with the 40 MHz transducer are presented and follow a similar trend. The spectral slopes measured using the 20 MHz transducer decrease from 0.9 dB/MHz for the untreated cells to 0.65 dB/MHz for the treated cells (30 h time point) and from 0.3 dB/MHz to 0.01 dB/MHz (30 h time point) using the 40 MHz transducer. Differences in the spectral slopes were detected 17 h after treatment.

The IBCs for the 20 MHz and the 40 MHz transducers are plotted as a function of treatment time in Fig. 7. For the 20 MHz data, an increase in the backscattered

energy between treated and untreated cells was measured, starting 6 h after treatment, reaching a maximum of $4.0 \cdot 10^{-3} \text{ sr}^{-1} \text{ mm}^{-1}$ at 30 h after treatment ($7.0 \cdot 10^{-4} \text{ sr}^{-1} \text{ mm}^{-1}$ before treatment) and decreases after 30 h. This trend is not observed for the 40 MHz data, presented in Fig. 7b, for which there are small differences between the treated and untreated cell samples, even though it is the exact same sample that the two transducers imaged.

To evaluate the significance of the differences between parameters measured at two different treatment times (3 h and 24 h) and between treated and untreated cell samples, an analysis of variance (ANOVA) was performed. Tested were estimates derived from treated and untreated cell samples at both treatment times. Table 3 shows the p -values estimated from the ANOVA. “SS20” in Table 3 refers to spectral slope obtained from 20 MHz data and IBC40 corresponds to the IBCs obtained from the 40 MHz data. T1 indicates that estimates from the treatment experiment at three hours were used, whereas U2 refers to estimates obtained from an untreated-24 h cell sample. Results stated in Table 3 demonstrate that parameter estimates of untreated cells obtained with the 20 MHz and 40 MHz transducer vary without statistical significance between the two treatment times (with exception of the IBC of the 40 MHz data). Signif-

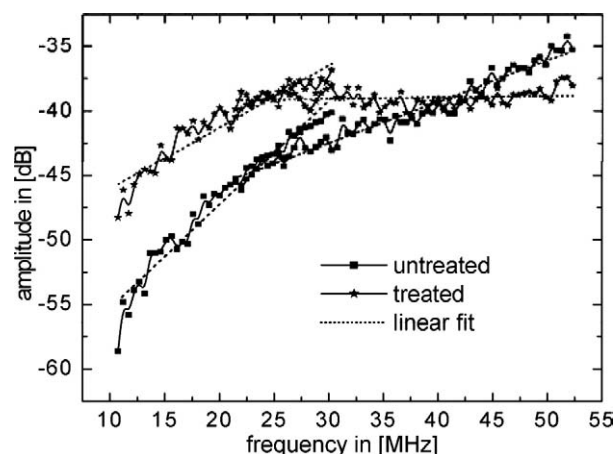


Fig. 5. Normalized power spectra of ultrasound backscatter signals from untreated (square) and 30 h treated (asterisk) HEP-2 cells at 20 and 40 MHz, with corresponding linear fits.

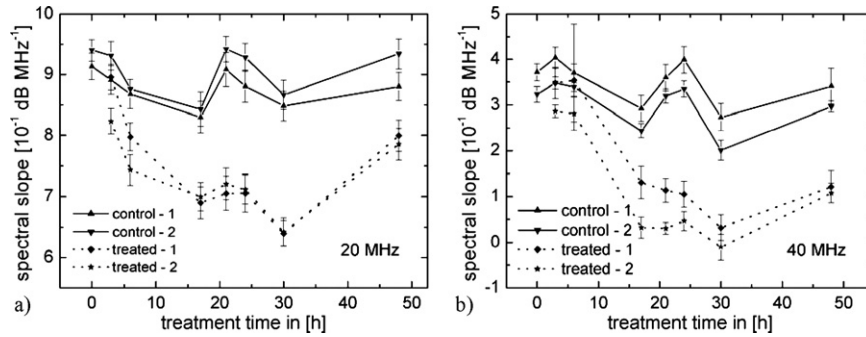


Fig. 6. Slope of normalized power spectrum for samples containing treated and untreated HEP-2 cells using the 20 MHz transducer (a) and the 40 MHz transducer (b).

icant deviations were observed for parameters obtained at 3 h and 24 h from treated cells. A p -value < 0.05 was also observed between treated and untreated cells at the two time points.

Figure 8 displays the corresponding maximum wavelet coefficients (MWC) as a function of treatment time. The MWC is the wavelet coefficient with the maximum amplitude estimated over all scaling factors and all scanning positions of the analyzing wavelet along the signals. Using the MWC of the 20 MHz data, the treated and untreated cells can be clearly differentiated. The data recorded using the 40 MHz transducer cannot differentiate between the two conditions. The mean scaling factors (MSF) of the MWC are plotted in Fig. 9. For both transducers, significant differences can be detected starting at 17 h of treatment. The scaling factors of the wavelet transformed increase over treatment time for treated HEP-2 cells by 10% for the 20 MHz transducer and 20% for the 40 MHz transducer, whereas the control samples show a variation of only 4% around the mean value (Fig. 9). The scaling factors for treated cells increase significantly after six hours and this suggests a correlation with the cell structural changes caused by the camptothecin treatment. Using the scaling factors where the maximum wavelet coefficients occur in the results of

the CWT, differentiation between treated and untreated cell samples is possible. Although the scaling factors of the MWC increased as a function of treatment time, the spectral slope estimates decreased for both transducers. Spectral slope values decrease when scaling factors of MWC increase. Variations of the wavelet analysis-based parameters were analyzed using ANOVA, corresponding to the analysis performed with the results of the spectral analysis. The obtained p -values are shown in Table 4. MSF20 and MSF40 represent the results of the MSF estimated from the 20 MHz and 40 MHz data, respectively. Maximum wavelet coefficients of 20 MHz and 40 MHz data belong to MWC20 and MWC40, respectively. According to Table 4, results obtained from treated and untreated cells at the 3 h time point do not show significant differences, whereas after 24 h, p -values between the two conditions are below the significance level of $p = 0.05$. Statistically significant differences were also detected between 3 h and 24 h of treatment.

DISCUSSION

The duration of exposure to the drug for which changes in the intensity of the backscattered sound were measured (Fig. 4) coincided with duration of exposure

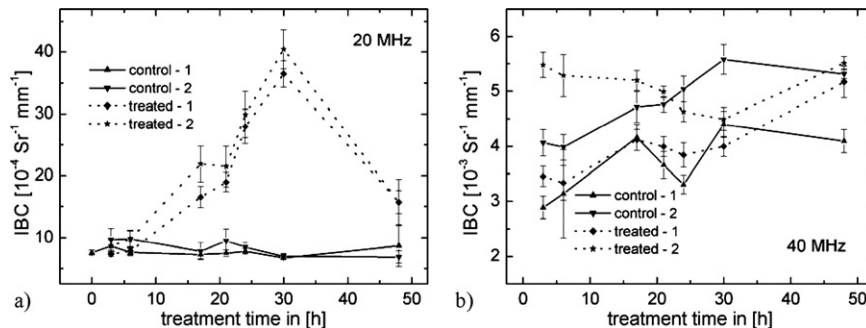


Fig. 7. IBCs of the ultrasound signals recorded from samples containing treated and untreated HEP-2 cells using the 20 MHz transducer (a) and the 40 MHz transducer (b).

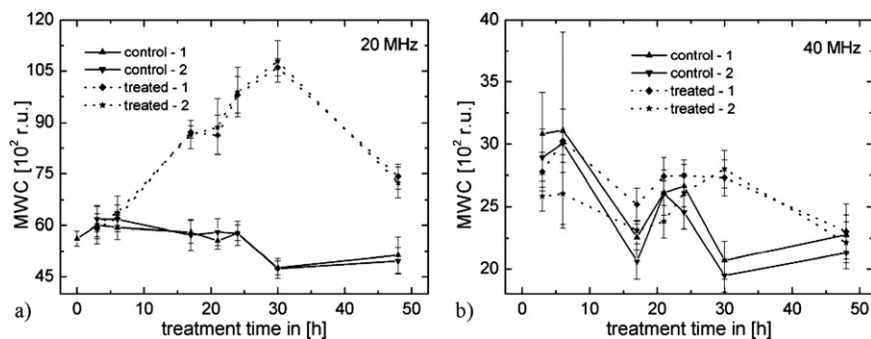


Fig. 8. Maximum wavelet coefficient of RF signals recorded from samples containing treated and untreated HEP-2 cells using the 20 MHz transducer (a) and the 40 MHz transducer (b).

for which changes in H&E histology were evident (Fig. 3). This demonstrates that structural changes at the cellular level that occur during apoptosis coincide in time with the variations in the ultrasonic backscatter properties.

The IBCs, the maximum wavelet coefficients and other intensity or energy-related parameters could be used for quantifying backscatter increase with time after treatment seen in Fig. 4. Values of the IBCs estimated from the 20 MHz data increase as a function of time, starting pretreatment and reaching a maximum of $4.0 \cdot 10^{-3} \text{ sr}^{-1} \text{ mm}^{-1}$ 30 h after treatment (Fig. 7a). This increase of IBCs is similar to what was measured using cisplatin to treat acute myeloid leukemia (AML) cells (Kolios et al. 2002, 2003; Tunis et al. 2005). MWC estimated from the same data increased by 100% compared with the initial values with the maximum coinciding in time with the IBC values. The IBCs measured using the 40 MHz transducer showed no appreciable difference between treated and untreated cells as represented in the *p*-values provided in Table 3. A similar behavior was observed for the MWC estimated from the 40 MHz data, which may be attributed to changes in frequency-dependent backscatter properties during apo-

ptosis. The slope of the normalized power spectrum reflects the frequency-dependent scattering. In our experiments, the slope of the normalized power spectrum decreased by 35% during the course of the treatment as presented in Fig. 6. This decrease in the spectral slope as a function of treatment time is the opposite trend compared with the increase in spectral slope seen from earlier experiments using AML cells and recent experiments with HeLa cells (Brand et al. 2005, 2008). However, in all of these experiments the cell histology indicates that structural changes associated with apoptosis occurred, even though there are subtle differences noted in the H&E histology. For example, in the experiments with the early AML (Czarnta et al. 1997; Kolios et al. 2002) and HeLa cells (Brand et al. 2005, 2008), large changes in cell structure were detected as early as 6 h after drug exposure (cisplatin) accompanied by clear cell fragmentation (apoptotic bodies). In the current experiments, large changes in structure occurred considerably after 6 h (Fig. 3). Moreover, although nuclear condensation occurs in all of these experiments, the cells in the HEP-2 samples seem intact (not forming apoptotic bodies) for much longer time periods than the other cells mentioned. Therefore, the increase or decrease of the spectral slopes

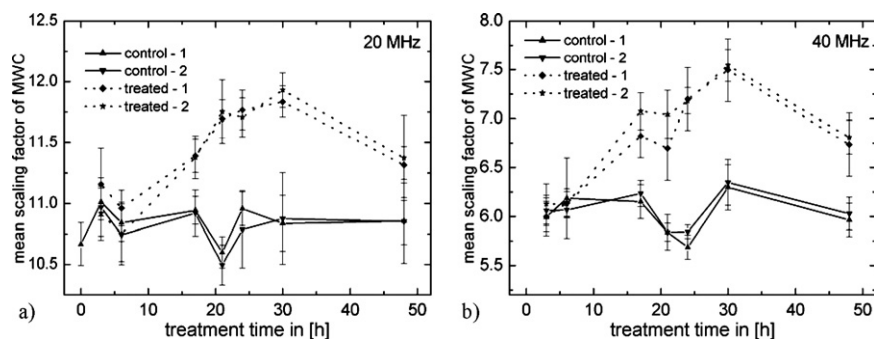


Fig. 9. Mean scaling factors of RF signals recorded from samples containing treated and untreated HEP-2 cells using the 20 MHz transducer (a) and the 40 MHz transducer (b).

Table 3. Results of ANOVA

	SS20	SS40	IBC20	IBC40
T1T2	$p < 0.05$	$p < 0.05$	$p < 0.05$	$p < 0.05$
U1T1	$p < 0.05$	$p < 0.05$	$p < 0.05$	$p < 0.05$
U2T2	$p < 0.05$	$p < 0.05$	$p < 0.05$	$p < 0.05$
U1U2	$p = 0.51$	$p = 0.5$	$p = 0.27$	$p < 0.05$

The p -values between parameter estimates obtained at different treatment times. T1 = 3h-treated; T2 = 24h-treated; U1 = 3h-control; U2 = 24h-control. SS20 = spectral slope 20 MHz-data; SS40 = spectral slope 40 MHz-data; IBC20 = integrated backscatter coefficients from 20 MHz data; IBC40 = IBC from 40 MHz data.

may reflect the phenotypic variation of the cells responding to the treatment, and may partially explain the differences in the ultrasound backscatter properties of treated cell lines. Finally, it should also be noted that the number of cells responding to the treatment varies according to the cell type: for the AML cells the majority of cells showed evidence of treatment response within 24 h, whereas in the current experiments, approximately 30–40% of the cells respond (data not shown). The data presented clearly demonstrate the subtleties associated with the detection of apoptosis using high-frequency ultrasound and the analysis based on the backscatter intensity: the same samples imaged with a 20 MHz transducer show a large change in backscatter intensity between treated and untreated cells, whereas at 40 MHz, no such change is detected. It should be noted that the same magnitudes in the IBCs estimated from the 40 MHz data could not be explained by an incomplete compensation of attenuation. Attenuation in the current study was calculated and accounted for at each treatment time. In Fig. 5 it can be seen that although the slopes of the normalized power spectra are different, the overall amplitude levels are similar for the 40 MHz data between treated and untreated samples. Because the IBCs integrate over the transducers bandwidth, frequency-dependent changes in intensity of the 40 MHz data were averaged out.

Experiments were repeated after two weeks with a fresh batch of cells. Quantitative acoustic parameters and histological assessed morphology showed very high reproducibility between the experiments. This can be seen in Figs. 6–9, in which a total of 26 cell samples were imaged and analyzed with two different transducers. Throughout all experiments, parameter values for “control-1” and “control-2” and also for “treatment-1” and “treatment-2” coincide. The reproducibility variations of parameter estimates observed in the control samples are hypothesized to be caused by structural changes in the cells that occur during the cell cycle.

In addition to traditional spectral analysis, the CWT was used to analyze backscatter signals. The MWC is

related to the energy of the backscattered signal and provides similar information as the IBC. By comparing Figs. 7 and 8, the same trend exhibited by the IBC is observed when plotting the MWC as a function of treatment time. The scaling factors of the MWC describe the periodicity of the analyzing wavelet and correspond to the estimates of the spectral slopes. When comparing estimates of the scaling factors of the MWC in Fig. 9 with the spectral slope estimates in Fig. 6, an opposite trend between treated and untreated cells is observed. This was expected, because the analyzing wavelet contains higher periodicity when scaling factors decrease. However, for untreated cell samples, the scaling factors of the MWC showed less variation as a function of time compared with values of the spectral slope. The scaling factors of the MWC computed for untreated HEP-2 cells vary by 0.7% around the mean value for the 20 MHz transducer and by 2% for the 40 MHz transducer. Spectral slope values, however, showed a variation of 6% for 20 MHz and 12% for the 40 MHz transducer. The smaller variations of the wavelet parameters compared with the traditional spectral analysis suggest that the precision of the measurement may be better for the wavelet analysis in quantitative ultrasound applications.

It should be mentioned that no compensation for transfer properties of the equipment was performed before wavelet analysis. A normalization of the signals to the properties of the analyzing wavelet occurs during the analysis. This leads to the conclusion that the choice of the mother wavelet is of importance and should be carefully considered in further applications. However, wavelet analysis does not contribute significantly different information than conventional spectral analysis, as implemented in this work. Because imaging of heterogeneous regions was not of concern in the current study, the time–localization advantage of the wavelet transform was not realized. However, it is expected that in clinical implementations of this technique for imaging of heterogeneous tissue, the advantages in terms of localizing responding regions will be exploited.

Table 4. Results of ANOVA

	SF20	SF40	MWC20	MWC40
T1T2	$p < 0.05$	$p < 0.05$	$p < 0.05$	$p = 0.64$
U1T1	$p = 0.71$	$p = 0.45$	$p = 0.48$	$p < 0.05$
U2T2	$p < 0.05$	$p < 0.05$	$p < 0.05$	$p < 0.05$
U1U2	$p = 0.18$	$p < 0.05$	$p < 0.05$	$p < 0.05$

The p -values between parameter estimates obtained at different treatment times. T1 = 3h-treated; T2 = 24h-treated; U1 = 3h-control; U2 = 24h-control. SF20 = scaling factors 20 MHz-data; SF40 = scaling factors 40 MHz-data; MWC20 = MWC from 20 MHz data; MWC40 = MWC from 40 MHz data.

ANOVA was performed on the estimates obtained by spectral and wavelet-based analysis. The resulting p -values are stated in Tables 3 and 4. The p -values exhibit significant differences ($p < 0.05$) for estimates of the spectral slope and the MSF between untreated cells and after 24 h of treatment. Significant differences between treated and untreated cell samples were detected other than for the IBC and MWC from data collected at 40 MHz. However, estimates of the spectral analysis permitted a differentiation as early as 3 h of treatment, which was not achieved with the wavelet analysis.

Compensating the time signals for transfer properties of the equipment and acoustic attenuation inside the cell samples before wavelet analysis may improve its performance and may also allow the differentiation at the early treatment times. In the current study wavelet analysis showed robustness and provided reliable parameter estimates, even without a precise calibration.

Relative differences of spectral slope and scaling factors between treated and untreated cells were similar for the measurements with 20 MHz and 40 MHz transducers. A more rigorous evaluation of the changes in attenuation during the treatment using a better technique (Taggart et al. 2007) will be a topic of future work. Brand et al. (2008) found that the attenuation of HeLa cells increased by 20% during the treatment. In this study, we found treatment-related attenuation variations of up to 40%.

Apart from the proposed experimental studies, simulations of ultrasound scattering are actively pursued. Because the spatial distribution and the size of the scattering objects influence the ultrasound backscatter signals, modeling of cell ensembles with different acoustic properties and scatterer spatial distribution will be performed and compared with the experimental data.

Acknowledgements—This research was undertaken, in part, thanks to funding from the Canada Research Chairs Program awarded to Michael Kolios. The authors would also like to acknowledge the financial support of the Whitaker Foundation (grants RG-01 to 0141), the Natural Sciences and Engineering Research Council (NSERC, CIHR grant 237962 to 2000), the Canadian Institutes of Health Research and the Ontario Premier's Research Excellence Awards (PREA 00/5 to 0730). The VisualSonics ultrasound bio microscope was purchased with the financial support of the Canada Foundation for Innovation, the Ontario Innovation Trust and Ryerson University. The authors would also like to thank Arthur Worthington and Anoja Giles for technical assistance.

REFERENCES

- Brand S, Weiss EC, Lemor RM, Kolios MC. Visualization of apoptotic cells using scanning acoustic microscopy and high frequency ultrasound. In Proceedings of the 2005 IEEE International Ultrasonics Symposium: 2005;882–885.
- Brand S, Weiss EC, Lemor RM, Kolios MC. High frequency ultrasound tissue characterization and acoustic microscopy of intracellular changes. *Ultrasound Med Biol* 2008;34(9):1396–1407.
- Bridal SL, Fornes P, Bruneval P, Berger G. Parametric (integrated backscatter and attenuation) images constructed using backscattered radio frequency signals (25–56 MHz) from human aortae in vitro. *Ultrasound Med Biol* 1997;23(2):215–229.
- Briggs A. Acoustic Microscopy. In Monographs on the Physics and Chemistry of Materials. Oxford: Clarendon Press, 1992.
- Cloutier G, Qin Z. Ultrasound backscattering from non-aggregating and aggregating erythrocytes—A review. *Biorheology* 1997;34(6):443–470.
- Czarnota GJ, Kolios MC, Vaziri H, Benchimol S, Ottensmeyer FP, Sherar MD, Hunt JW. Ultrasonic biomicroscopy of viable, dead and apoptotic cells. *Ultrasound Med Biol* 1997;23(6):961–965.
- Dancey J, Eisenhauer EA. Current perspectives on camptothecins in cancer treatment. *Br J Cancer* 1996;74(3):327–338.
- Donehower RC, Kaufmann SH. The current status of camptothecin analogues as antitumor agents. *J Nat Cancer Inst* 1993;85(4):221–291.
- Doonan F, Cotter TG. Morphological assessment of apoptosis. *Methods* 2008;44(3):200–204.
- Feleppa EJ, Lizzi FL, Coleman DJ, Yaremko MM. Diagnostic spectrum analysis in ophthalmology: A physical perspective. *Ultrasound Med Biol* 1986;12(8):623–631.
- Foster FS, Pavlin CJ, Harasiewicz KA, Christopher DA, Turnbull DH. Advances in ultrasound biomicroscopy. *Ultrasound Med Biol* 2000;26(1):1–27.
- Gaertner T, Jenderka K, Schneider H, Heynemann H. Tissue characterization by imaging of acoustical parameters. *Acoust Imaging* 1996;22:365–370.
- Georgiou G, Cohen F. A hope for a cheap and reliable automatic Diagnostic system for breast cancer. *IEEE Trans Ultrason Ferroelectr Freq Control* 2000;1311–1314.
- Georgiou G, Cohen FS. Tissue characterization using the continuous wavelet transform. Part I: Decomposition method. *IEEE Trans Ultrason Ferroelectr Freq Control* 2001;48(2):355–363.
- Graps A. An introduction to wavelets. *IEEE Comp Sci Eng* 1995;2(2):50–61.
- Huisman HJ, Thijssen JM, Wagener DJ, Rosenbusch GJ. Quantitative ultrasonic analysis of liver metastases. *Ultrasound Med Biol* 1998;24(1):67–77.
- Insana MF, Hall TJ. Characterising the microstructure of random media using ultrasound. *Phys Med Biol* 1990;35(10):1373–1386.
- Insana MF, Wagner RF, Brown DG, Hall TJ. Describing small-scale structure in random media using pulse-echo ultrasound. *J Acoust Soc Am* 1990;87(1):179–192.
- Jenderka KV, Millner R, Richter KP, Leitgeb N, Wach P. Ultrasound backscatter and tissue characterization. *Biomed Tech (Berl)* 1990;35(3):282–283.
- Jenderka KV, Gärtner T, Zacharias M, Heynemann H, Cobet US. System independent tissue typing of human testis and prostate. *Proceedings IEEE Ultrason Symp* 1999;2:1377–1380.
- Jones NL, Islur A, Haq R, Mascarenhas M, Karmali M, Perdue MH, Zanke BW, Sherman PM. *Escherichia coli* Shiga toxins induce apoptosis in epithelial cells that is regulated by the Bcl-2 family. *Am J Physiol Gastro Liver Physiol* 2000;278:G811–G819.
- Kaufmann SH, Peereboom D, Buckwalter CA, Svingen PA, Grochow LB, Donehower RC, Rowinsky EK. Cytotoxic effects of topotecan combined with various anticancer agents in human cancer cell lines. *J Natl Cancer Inst* 1996;88(11):734–741.
- Kolios MC, Czarnota GJ, Lee M, Hunt JW, Sherar MD. Ultrasonic spectral parameter characterization of apoptosis. *Ultrasound Med Biol* 2002;28(5):589–597.
- Kolios MC, Taggart L, Baddour RE, Foster SF, Hunt JW, Czarnota GJ, Sherar MD. An investigation of backscatter power spectra from cells, cell pellets and microspheres. *Proc IEEE Int Ultrason Symp* 2003;752–757.
- Li LH, Fraser TJ. Action of camptothecin on mammalian cells in culture. *Cancer Res* 1972;32(12):2643–2650.
- Lizzi FL, Ostromogilsky M, Feleppa EJ, Rorke MC, Yaremko MM. Relationship of ultrasonic spectral parameters to features of tissue microstructure. *IEEE Trans Ultrason Ferroelectr Freq Control* 1986;33:319–329.

- Lizzi FL, Astor M, Feleppa EJ, Shao M, Kalisz A. Statistical framework for ultrasonic spectral parameter imaging. *Ultrasound Med Biol* 1997a;23(9):1371–1382.
- Lizzi FL, Feleppa EJ, Astor M, Kalisz A. Statistics of ultrasonic spectral parameters for prostate and liver examinations. *IEEE Trans Ultrason Ferroelectr Freq Control* 1997b;44(4):935–942.
- Lizzi FL. Ultrasonic scatterer-property images of eye and prostate. *Proc IEEE Ultrason Symp* 1997c;1109–1117.
- Lizzi FL, Greenebaum M, Feleppa EJ, Elbaum M, Coleman DJ. Theoretical framework for spectrum analysis in ultrasonic tissue characterization. *J Acoust Soc Am* 1983;73(4):1366–1373.
- Lizzi FL, King DL, Rorke MC, Hui J, Ostromogilsky M, Yaremko MM, Feleppa EJ, Wai P. Comparison of theoretical scattering results and ultrasonic data from clinical liver examinations. *Ultrasound Med Biol* 1988;14(5):377–385.
- Lu ZF, Zagzebski JA, Lee FT. Ultrasound backscatter and attenuation in human liver with diffuse disease. *Ultrasound Med Biol* 1999;25(7):1047–1054.
- Madsen EL, Dong F, Frank GR, Garra BS, Wear KA, Wilson T, Zagzebski JA, Miller HL, Shung KK, Wang SH, Feleppa EJ, Liu T, O'Brien WD Jr, Topp KA, Sanghvi NT, Zaitsev AV, Hall TJ, Fowlkes JB, Kripfgans OD, Miller JG. Interlaboratory comparison of ultrasonic backscatter, attenuation, and speed measurements. *J Ultrasound Med* 1999;18(9):615–631.
- Mamou J, Oelze ML, O'Brien WD, Zachary JF. Identifying ultrasonic scattering sites from three-dimensional impedance maps. *J Acoust Soc Am* 2005;117(1):413–423.
- Nair A, Kuban BD, Obuchowski N, Vince DG. Assessing spectral algorithms to predict atherosclerotic plaque composition with normalized and raw intravascular ultrasound data. *Ultrasound Med Biol* 2001;27(10):1319–1331.
- Nicholas D. Evaluation of backscattering coefficients for excised human tissues: Results, interpretation and associated measurements. *Ultrasound Med Biol* 1982;8:17–28.
- Oelze ML, Zachary JF, O'Brien WD Jr. Differentiation of tumor types in vivo by scatterer property estimates and parametric images using ultrasound backscatter. *IEEE Trans Ultrason Ferroelectr Freq Control* 2003;1:1014–1017.
- Oelze ML, O'Brien WD Jr. Improved scatterer property estimates from ultrasound backscatter for small gate lengths using a gate-edge correction factor. *J Acoust Soc Am* 2004a;116(5):3212–3223.
- Oelze ML, O'Brien WD Jr, Blue JP, Zachary JF. Differentiation and characterization of rat mammary fibroadenomas and 4T1 mouse carcinomas using quantitative ultrasound imaging. *IEEE Trans Med Imaging* 2004b;23(6):764–771.
- Oelze ML, Zachary JF, O'Brien WD Jr. Parametric imaging of rat mammary tumors in vivo for the purposes of tissue characterization. *J Ultrasound Med* 2002;21(11):1201–1210.
- Oelze ML, O'Brien WD Jr. Application of three scattering models to characterization of solid tumors in mice. *Ultrasound Imaging* 2006;28(2):83–96.
- Romijn RL, Thijssen JM, van Delft JL, de Wolff-Rouendaal D, van Best J, Oosterhuis JA. In vivo ultrasound backscattering estimation for tumor diagnosis: An animal study. *Ultrasound Med Biol* 1989;15(5):471–479.
- Saied A, Laugier P. High-resolution ultrasonography for analysis of age- and disease-related cartilage changes. *Method Mol Med* 2004;101:249–265.
- Shinka BK. Topoisomerase inhibitors. A review of their therapeutic potential in cancer. *Drugs* 1995;49:11–19.
- Silverman RH, Lizzi FL, Ursea BG, Rondeau MJ, Eldeen NB, Kalisz A, Lloyd HO, Coleman DJ. High-resolution ultrasonic imaging and characterization of the ciliary body. *Invest Ophthalmol Vis Sci* 2001;42(5):885–894.
- Silverman RH, Rondeau MJ, Lizzi FL, Coleman DJ. Three-dimensional high-frequency ultrasonic parameter imaging of anterior segment pathology. *Ophthalmology* 1995;102(5):837–843.
- Taggart LR, Baddour RE, Giles A, Czarnota GJ, Kolios MC. Ultrasonic characterization of whole cells and isolated nuclei. *Ultrasound Med Biol* 2007;33(3):389–401.
- Taron M, Plasencia C, Abad A, Martin C, Guillot M. Cytotoxic effects of topotecan combined with various active G2/M-phase anticancer drugs in human tumor-derived cell lines. *Invest New Drugs* 2000;18(2):139–147.
- Tunis AS, Czarnota GJ, Giles A, Sherar MD, Hunt JW, Kolios MC. Monitoring structural changes in cells with high frequency ultrasound signal statistics. *Ultrasound Med Biol* 2005;31(8):1041–1049.
- Turnbull DH, Wilson SR, Hine AL, Foster FS. Ultrasonic characterization of selected renal tissues. *Ultrasound Med Biol* 1989;15(3):241–253.
- Ursea R, Coleman DJ, Silverman RH, Lizzi FL, Daly SM, Harrison W. Correlation of high-frequency ultrasound backscatter with tumor microstructure in iris melanoma. *Ophthalmology* 1998;105(5):906–912.
- Vogt M, Knüttel A, Hoffmann K, Altmeyer P, Ermert H. Comparison of high frequency ultrasound and optical coherence tomography as modalities for high resolution and non invasive skin imaging. *Biomed Tech (Berl)* 2003;48(5):116–121.
- Waters KR, Bridal SL, Cohen-Bacrie C, Levrier C, Forners P, Laugier P. Parametric analysis of carotid plaque using a clinical ultrasound imaging system. *Ultrasound Med Biol* 2003;29(11):1521–1530.
- Worthington AE, Sherar MD. Changes in ultrasound properties of porcine kidney tissue during heating. *Ultrasound Med Biol* 2001;27(5):673–682.
- Yu FTH, Cloutier G. Experimental ultrasound characterization of red blood cell aggregation using the structure factor size estimator. *J Acoust Soc Am* 2007;122(1):645–656.